1.48 INTRA-FARM WIND SPEED VARIABILITY OBSERVED BY NACELLE ANEMOMETERS IN A LARGE INLAND WIND FARM

Hoonill Won[1]

National Wind Institute, Texas Tech University, Lubbock, Texas 79409, U.S.A.

Song-Lak Kang

Department of Geosciences, Texas Tech University, Lubbock, Texas 79409, U.S.A.

1. INTRODUCTION

Concerning that a large inland wind farms are often constructed over heterogeneous surfaces such as mountainous areas, it is critical to understand the significance of variability of intra-farm wind flows as they influence power production. In the research, we studied the spatial and temporal characteristics of wind speed measurements by nacelle anemometers at 274 wind turbines in a large wind farm of an area of about 20 km by 20 km. Our hypothesis is that spatial variability of wind speed in a wind farm on scales ≤ O(10 km) is associated with temporal variability on scales ≤ O(10 h) [Manwell et al.,2010; Orlanski,1975; Stull,1988]. We also discuss the intra-farm spatial and temporal variability of wind speed in terms of the accuracy of wind power production estimation.

2. DATA

We used wind speed data measured from 3-cip nacelles anemometers installed on the wind turbine nacelles in side of a large wind farm whose area covers about 20 km by 20 km described in Figure 1 indicating that turbines are situated in a mountainous region. The wind farm contains 274 wind turbines and 221 out of them have 69 m hub height and the rest have 80 m [Liu et al., 2011; Wan et al., 2010; Zhang et al., 2014]. The data are 15-minute averaged time series from 1 January to 30 November 2012. As Table 1 described, the percentage of the missing points out of total 11-month time series is about 14 % which is the obstacle to use whole data set. For seasonal analyses we divided from March to May as Spring, from June to August as Summer, from September to November as Fall and from January to February (because we were not provided December data) following convention. Table 1 also indicates that spring and fall has much more missing points than summer and winter in general. For selecting time series data used, 11-month time series are separated into 44 week periods and with the criteria of selecting the periods whose longest consecutive missing length is less than or equal to 3 hours, total 10 weeks were selected. Each 5 weeks are from winter and summer seasons and their statistics are described in table 2. Figure 2 indicates different main wind directions between in winter and summer in the wind farm from the meteorological tower A09 depicted in Figure 1.

3. ANALAYSUS RESULTS

3.1. Dominant time scales of wind speed fluctuations

To investigate the temporal characteristics of the seasonal intra farm wind speed, we applied the Fourier analyses on the selected 1-week time series with 15-minute interval of each 5 weeks from winter and summer which its time scale on spectrum would be from half an hour (due to Nyquist frequency) to 168 hours. Because Fourier spectral analysis requires the complete series of the data, we applied interpolation methods on missing points in selected time series as shown. Figure 3 (b) indicates that the type of the interpolation method doesn't affect the result of Fourier spectrum much especially in terms of spectral peaks. Individual gray lines in Figure 3 (a) indicates Fourier spectra from each wind turbines in one week and the solid blue lines and error bars the average and the standard deviation of them respectively. Figure 4 shows the averaged spectra for

[1] Corresponding author address: Hoonill Won, Texas Tech University, Nation Wind Institute, Lubbock, TX 79409-3155 ; e-mail: hoonill.won@ttu.edu

winter and summer. The blue solid line and the error bars indicates the average of five 1-week spectra and the standard deviation of them for each season. From Figure 4, we can see that diurnal cycle is the dominant scale for wind flow during summer while the larger scales of 40 to 50 hour dominate winter wind flow.

3.2. Spatial correlations between the intra-farm time series

In order to define the spatial variability of wind flow in side of the wind farm, we calculated the Pearson's product-moment correlation coefficient, $\rho(M_r, M_i)$, between the time series from the reference turbines, M_r and the *i* th wind turbine, M_i at each week:

$$\rho(M_r, M_i) = \frac{cov(M_r, M_i)}{\sigma_{M_r}\sigma_{M_i}}, \quad (1)$$

where *cov* is the covariance between M_r and M_i, and σ the temporal standard deviation of M_r or M_i over the week. The reference turbines at each week are depicted in Table 1.

Figure 5 shows the correlation coefficient, $\rho(M_r, M_i)$, with distance from the reference turbines for winter (a) and summer (b). For both winter and summer, correlation coefficients with distance decrease, but the slope is much steep for summer than winter. The decrease with distance could be due to local heterogeneity between two turbines and we can say that steeper slope of decrease can be caused by more spatial variability. For the reasons, wind flows during summer in this wind farm could be more spatially variable than those during winter.

In Figure 7, temporal low-pass filter, which was descried in Figure 6, was applied for each five 1-week time series for both winter and summer and the correlation coefficients, $\rho([M_r]_P, [M_i]_P)$, with low-pass filtered time series $[M_r]_P$ and $[M_i]_P$ were computed with distance. With the cut-offf scales of 3, 6, 12 and 24 hours, spatial correlation coefficients are improved with increasing temporal cut-off scales. It indicates that spatial variability of wind flow in a wind farm on scales ≤ O(10 km) is related with temporal variability on scales ≤ O(10 h) which we hypothesized in the instruction. Especially in Figure 7 (b), correlation coefficients are not fully recovered even after 24-hour scale low-pass filter. It indicates that there are some non-linearity existing in wind flow in summer which cannot be removed by linear low-pass filter.

3.3. Probability density functions (PDFs) of temporal velocity increments

To investigate the temporal change of the wind speed time series from the nacelle anemometers, we applied the probability density functions of velocity increments on each selected 1-week period as shown in Equation (2) below:

$$\delta M(\tau) = M(X_i, t+\tau) - M(X_i, t), \quad (2)$$

Figure 8 shows the PDFs of velocity increments with τ = 15 minute for each week during winter as well as winter. And Figure 9 indicates the PDFs of velocity increments for winter and summer with τ = 15 minute, 30 minute, 3 hour, 6 hour, and 12 hours. PDFs of velocity increments in both Figure 8 and 9 presents heavier tails in negative side relative to Gaussian distribution and that negative skewness is more significant on summer. As τ increases, the PDFs become closer to Gaussian, while those still show the negative skewness up to $\tau \leq 3$ h. The results indicate that rapid and sudden decreases of wind speed, which is usually called as the ramp-down are more frequent than ramp-up events over a time period ≤ 3 h, which is more significant during summer than during winter.

3.4. Diurnal variation of wind speed

Figure 10 presents the intra-farm spatial variability of wind speed as a function of the time of a day, using all the one-day time series in side of the wind farm from the thirty-five days of each selected five weeks for winter and summer. First, for each day we averaged wind speed over the wind farm along the diurnal cycle: $\langle M \rangle$ indicates the spatially averaged wind speed over a whole wind farm with diurnal cycle and $\{\langle M \rangle\}$ is calculated by averaging the time series of the spatially averaged wind speed over the thirty-five days for each season. Also the standard deviation σ_S of all the time series over the wind farm from the wind

speed *M* and temporal average of the spatial standard deviation with thirty five days, $\{\sigma_s\}$, are calculated to investigate the intra-farm spatial variability of the diurnal variation of wind speed for each season as shown in Fig. 10. It shows the intra-farm variability is more significant in the nighttime than in the daytime and when the mean flow becomes stronger, the spatial variation of smaller-scale flow would decrease. Conversely, when the mean flow becomes weaker, the spatial variations increase [Kang and Lenschow, 2014].

3.5. Intra-farm wind speed variability and wind power production

We estimated the wind power production with and without intra-farm wind speed variability for each season. The individual wind power estimation, e, was calculated with the equation (3) and total wind farm power estimation was with equation (4):

$$e = \frac{1}{2} \times \rho \times C_P \times A \times M^3, \quad (3)$$

$$e_{tot} = \sum_{i=1}^{N} e_i, \quad (4)$$

M here is qualified 1-week wind speed time series from each selected wind turbine with 15 minute intervals. We assumed ρ as sea level air density and C_P as the theoretical maximum capacity factor which is 0.593. *A* is a typical rotor disc area of 3848 m^2 [Burton et al., 2011; Manwell et al., 2010; Poore and Lettenmaier, 2003]. N is the number of the selected wind turbine for each week in each season. Also to calculate the wind power production without considering intra-fam wind speed variability, we used equation (5) and compare it with e_{tot} :

$$E = \frac{1}{2} \times \rho \times C_P \times A \times \langle M \rangle^3 \times N \quad (5)$$

For wind power estimation, we set that the cut-in speed of 3.0 $\mathrm{m\ s^{-1}}$, the rated speed of 11.5 $\mathrm{m\ s^{-1}}$, and the cut-out speed of 27.6 $\mathrm{m\ s^{-1}}$ and the rated power is 1.5 MW [Poore and Lettenmaier,2003]. As shown in Figure 11, for both winter and summer, for greater production above 200 MW, wind farm power calculation without considering intra-farm wind speed variability is overestimated than that with considering wind speed variability.

4. CONCLUSION

The intra-farm variability of wind speed in both spatial and temporal aspects were investigated utilizing qualified five 1-week wind speed time series by nacelle anemometers at selected wind turbines from total 274 turbines in a large wind farm over an area of about 20 × 20 km2.

During summer influence of diurnal variation is the most significant factor on wind flow in temporal scale, while the spectral peak during winter is located at longer than 24 hours.

Correlation coefficients are larger during winter than during summer with as well as without low-pass filter. Also, the wind speed temporal intermittency is more significant during summer than during winter.

Rapid wind ramp-down events are much more frequent, on temporal scales ≤ 3 h, during both winter and summer than a Gaussian PDF suggests and the wind farm power forecast may be overestimated without considering intra-fam wind speed variability especially for large wind power production.

ACKNOWLEDGEMENTS

We appreciate Drs. Yubao Liu and Yuewei Liu at the Research Application Laboratory of the National Center for Atmospheric Research for providing the nacelle anemometer data. We also appreciate Dr. Andrew Swift in National Wind Institute in Texas Tech University for his support.

REFERENCES

Burton T., Sharpe D., Jenkins N., Bossanyi E., 2011. Wind Energy Handbook, Second Ed. John Wiley & Sons LTD, United Kingdom, 4, 41 – 43, 110.

Kang S.L., Lenschow D.H., 2014. Temporal evolution of low-level winds induced by two-dimensional mesoscale surface heat-flux heterogeneity. Bound.-Layer Meteorol.151, 501-529. DOI 10.1007/s10546-014-9912-8

Liu Y., Warner T., Liu Y. , Vincent C., Wua W., Mahoney B., Swerdlin S., Parks K., Boehnert J., 2011. Simultaneous nested modeling from the synoptic scale to

the LES scale for wind energy applications. J. Wind Eng. Ind. Aerodyn. 99, 308-319. DOI: 10.1016/j.jweia.2011.01.013

Manwell J.F., McGowan J.G., Rogers A.L., 2010. Wind Energy Explained: Theory, Design and Application. Second ed. John Wiley & Sons LTD, United Kingdom, 28, 37.

Orlanski I., 1975. A rational subdivision of scales for atmospheric processes. Bull. Am. Meteorol. Soc. 56, 527–530.

Stull R., 1988. An Introduction to Boundary Layer Meteorology. Springer, 20.

Wan Y-H., Ela E., Orwig K., 2010. Development of an Equivalent Wind Plant Power-Curve. WindPower 2010 Conference, Dallas, Texas May 23-26, 2010 NREL/CP-550-4

Zhang J., Chowdhury S., Hodge B.-M., 2014. Analyzing effects of turbulence on power generating using wind plant monitoring data. the AIAA Science and Technology Forum and Exposition, National Harbor, Maryland, January 13-17, 2014. NCEP/CP-5D00-609898146

Poore R., Lettenmaier T., 2003. Alternative Design Study Report: WindPACT Advanced Wind Turbine Drive Train Designs Study. November 1, 2000 – February 28, 2002. Subcontractor Report. National Renewable Energy Laboratory, Golden, Colorado, 21. NREL/SR-500-33196

FIGURES AND TABLES

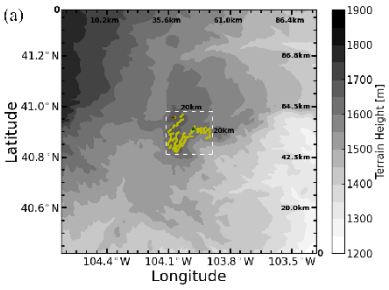

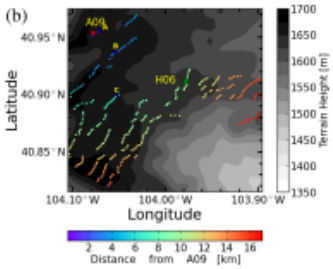

Figure 1. Locations of 274 wind turbines, two meteorological towers, A09 and H06 in the study wind farm. The color-filled contours are the terrain heights (a) in and (b) around the wind farm. The distance of each wind turbine from A09 is marked with the color of each dot at the turbine location. Also indicated are the reference wind turbines (A, B, and C) used for the correlation coefficients presented in Figs. 6-8.

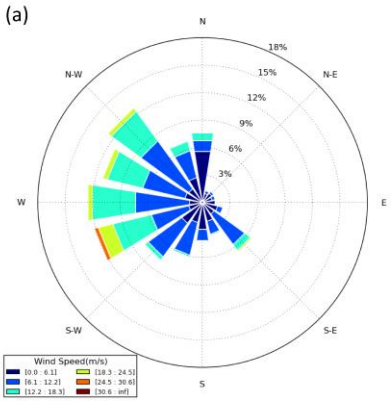

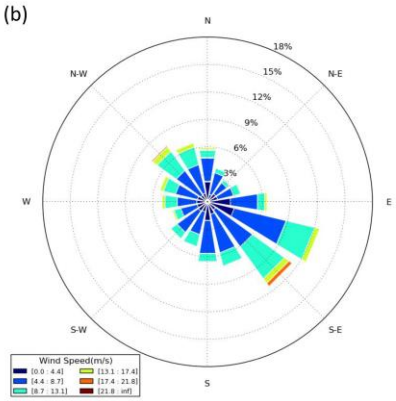

Figure 2. Wind roses derived from wind measurements at the height of 80 m on the A09 meteorological tower during the (a) winter and (b) summer seasons.

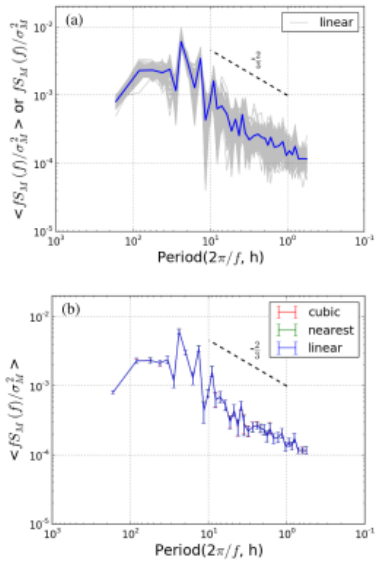

Figure 3. (a) An example of the composite spectrum $\langle fS_M(f)/\sigma_M^2 \rangle$ over the wind farm (thick blue line) and the individual spectra $fS_M(f)/\sigma_M^2$ used for the composite spectrum (thin gray lines). (b) The composite spectra of one-week time series filled with the three different interpolation methods: cubic, nearest, and linear. The error bars represent the standard deviations of the composite spectrum over the individual spectra. The reference spectral slop of $f^{-2/3}$ is plotted with the black dashed line.

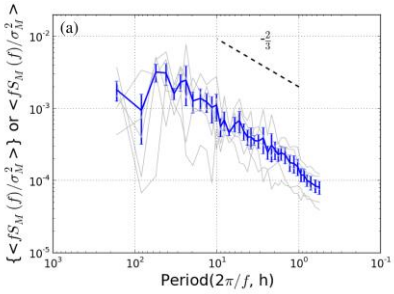

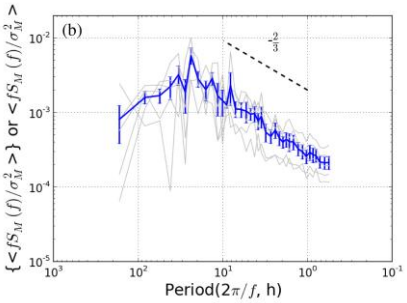

Figure 4. Composite spectra $\{\langle fS_M(f)/\sigma_M^2 \rangle\}$ (blue line) of nacelle anemometer wind speed for the (a) winter and (b) summer seasons. The gray lines are the spectra $\langle fS_M(f)/\sigma_M^2 \rangle$ of all the five, one-week time series of wind speed for each season. The error bars represent the standard deviations of $\{\langle fS_M(f)/\sigma_M^2 \rangle\}$ over the five $\langle fS_M(f)/\sigma_M^2 \rangle$. The reference spectral slop of $f^{-2/3}$ is plotted with the black dashed line.

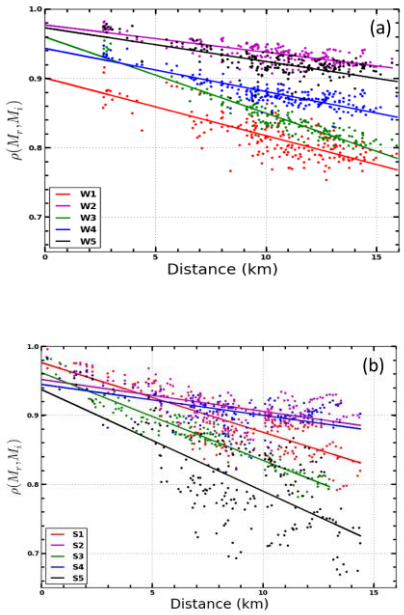

Figure 5. Correlation coefficients (symbols) of the nacelle anemometer time series between at the reference wind turbine and all the selected wind turbines for the five weeks of the (a) winter, (b) summer seasons. The linear regression lines are obtained using the least square method.

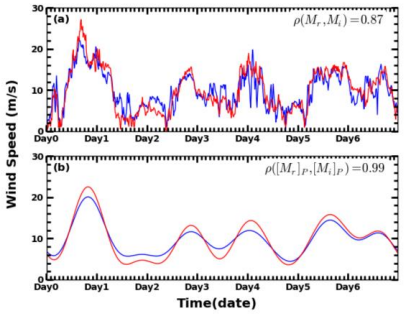

Figure 6. Comparison of (a) 15-min averaged nacelle anemometer time series at a reference wind turbine M_r (blue line) and at an ith wind turbine M_i (red line) over a week. Also compared are the low-pass filtered fields $[M_r]_P$ (blue lines) and $[M_i]_P$ (red lines) with a cutoff time scale *P* = 24 h. Here, the correlation coefficient ρ between the two time series is presented.

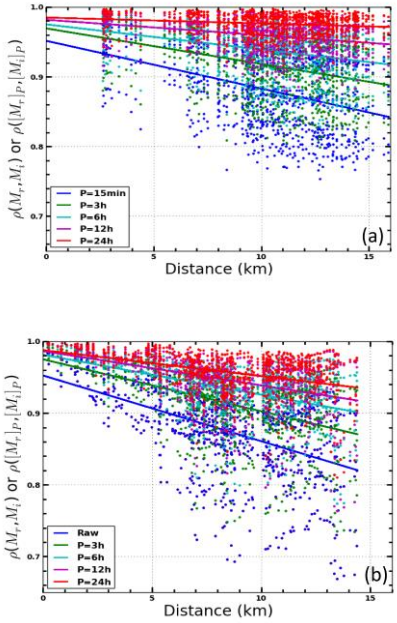

Figure 7. Correlation coefficients $\rho(M_r, M_i)$ (blue) between the time series at the reference wind turbines and the other wind turbines as a function of the distance between them for the (a) winter and (b) summer seasons. Coefficients $\rho([M_r]_P, [M_i]_P)$ are also obtained after the time series being low-pass filtered with the cutoff time scales P of 3 h (green), 6 h (cyan), 12 h (magenta), and 24 h (red). The lines are the linear regression lines whose colors match with the colors of the symbols.

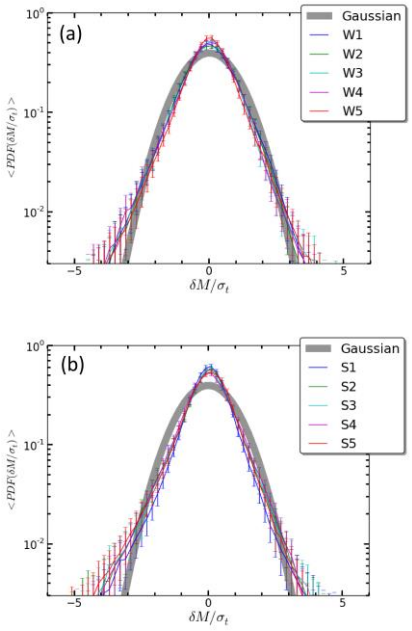

Figure 8. The spatial composites <PDF>s of the probability density functions (PDFs) of the velocity increments $\delta M(\tau) = M(x_i, y_i, t+\tau) - M(x_i, y_i, t)$ over the wind farm for every week (a) in the winter season, and (b) in the summer season. $M(x_i, y_i, t)$ is a one-week time series of nacelle wind speed at a wind turbine located at $\boldsymbol{X_i} = (x_i, y_i)$. The τ is the time lag and here is 15 min. For each one-week time series, the velocity increments are normalized with the standard deviation of wind speed over the time series: $\delta M/\sigma_t$. The error bars represent the spatial standard deviations σ_s of the <PDF>s over the PDFs at all the participating wind turbines for each week. The thick gray solid lines represent the Gaussian PDFs.

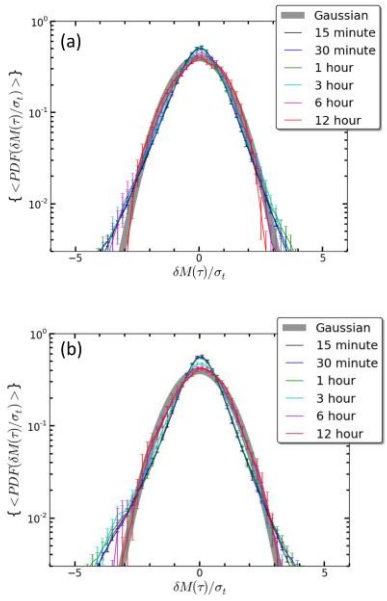

Figure 9. The ensemble-averaged PDFs $\{\langle \mathrm{PDF} \rangle\}$ as a function of the normalized velocity increment $\delta M(\tau)/\sigma_t$ with the temporal standard deviation σ_t over each one-week time series for (a) the winter and (b) summer seasons. The time lag τ varies, at 15 min, 30 min, 1 h, 3 h, 6 h, and 12 h. The thick gray solid lines represent the Gaussian PDFs. For each season and each time lag, at each $\delta M(\tau)/\sigma_t$, the standard deviation σ_{ts} marked with the error bar quantifies the temporal variability of $\{\langle \mathrm{PDF} \rangle\}$ over the five <PDF>s.

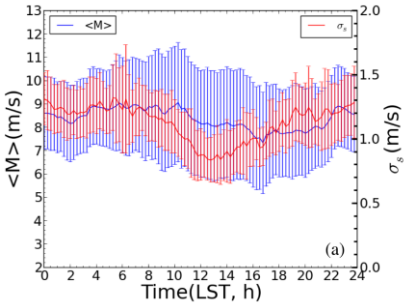

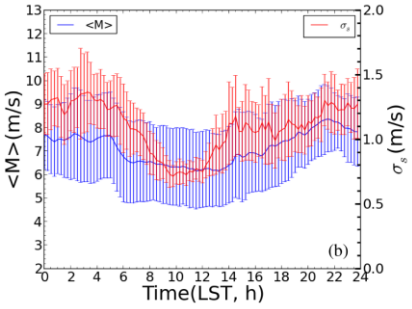

Figure 10. The intra-farm averaged wind speed $\langle \mathrm{M} \rangle$ and the standard deviation σ_s of the intra-farm wind speeds obtained as a function of the time of a day during (a) winter and (b) summer.

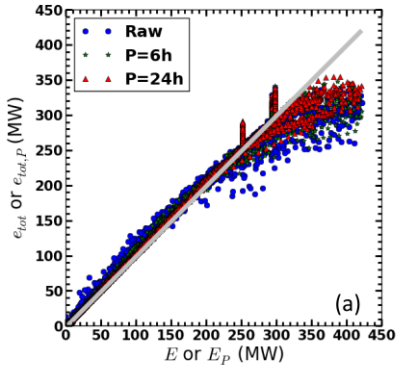

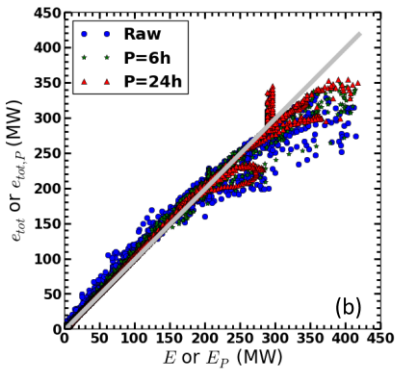

Figure 11. Total power over the wind farm considering the intra-farm variability with raw data e_{tot} and low-pass filtered data $e_{tot,P}$ (P=6 and 3h), and total power without considering the intra farm variability with raw data *E* and low-pass filtered data *Ep* for (a) winter and (b) summer.

Table 1

The percentage of missing data points and the median value of the longest periods of consecutive missing data points of the nacelle anemometer time series at all the 274 wind turbines for each month.

Month	Missing points/Total points (%)	Median of the longest periods of consecutive missing data points (hours)
January	2	0.75
February	10	2.75
March	22	10
April	32	43.25
May	7	4.25
June	15	1.25
July	11	4.75
August	7	2.25
September	16	6.25
October	10	5.5
November	20	13
Total 11 months	14	3.75

Table 2

For each study week, the number *N* of nacelle anemometers whose time series have the longest period of consecutive missing points ≤ 3 hours, the percentage *R* of missing points out of the total data points, the median value *Me* of the longest periods of consecutive missing points over the 274 anemometer time series. The reference turbines, the locations of which are marked in Fig. 1, are used in 3.2.

Season	Week	*N*	*R* (%)	*Me* (h)	Reference turbine
Winter	W1	196	0.9	0.75	A
	W2	199	0.7	0.75	A
	W3	168	3	2.75	A
	W4	199	0.2	0.25	A
	W5	199	2	1.00	A
Summer	S1	195	0.3	0.25	B
	S2	193	1.6	1.25	B
	S3	137	1.8	0.75	C
	S4	137	1.5	1.25	B
	S5	198	1.4	1.75	B